RSC Advances

PAPER

View Article Online
View Journal | View Issue

Cite this: *RSC Adv.*, 2017, **7**, 15228

Low electrical resistivity of a graphene–AgNHPs based ink with a new processing method

Piao Liu,[ab] Quanzhong Tang,[b] Hua Liu[b] and Anxian Lu*[a]

Received 9th January 2017
Accepted 2nd March 2017

DOI: 10.1039/c7ra00309a

rsc.li/rsc-advances

The purification and separation of nano-Ag particles is difficult because of the small size, it restricts the applications of nano-Ag. In this study, the AgNHPs solution was purified and separated with a membrane separation-centrifugation cleaning method, for use as the ink of printed electronics. Meanwhile, we prepared inkjet-printed patterns of conductive inks consisting of AgNHPs and graphene (GE) in different contents. It is found that high dispersity and low electrical resistivity of AgNHPs inks can be obtained by using membrane separation-centrifugation cleaning method. The AgNHPs particles show excellent dispersion and the electrical resistivity of the AgNHPs solution is 11.2×10^{-6} Ω cm at 150 °C, it increases the electrical conductivity of GE–AgNHP. It is also found that GE can significantly improve the electrical conductivity of the patterns when sintering is done at relatively low temperatures. When the GE content is 0.15 mg mL^{-1}, the resistivity is the lowest. For instance, when sintering is done at 150 °C, the resistivity is 2.5×10^{-6} Ω cm that is 13% of that of the AgNHPs conductive ink; after sintering at 50 °C, this ratio is 2%. This study on GE–AgNHPs conductive inks sintered at low temperatures should further the development of flexible touch screens.

Introduction

Silver is a highly conductive metal with a good oxidation resistance and is used widely as a conductive material.[1–3] Especially, nanoscale silver is used for printed electronics inks, that can be used to form high-precision conducting circuits on various flexible substrates, including radio-frequency identification (RFID) devices, smart labels, organic light-emitting diode (OLED) displays, flexible printed circuits (FPCs)[4–8] and flexible energy-related devices.[9,10] However, it remains a challenge to use conductive inks on substrates that cannot withstand high sintering temperatures, such as paper[1,4] and PET.[6]

Nanoscale Ag materials with spherical, cubic, flake-like, thread-like, and branch-like morphologies show special properties. Silver nanoparticles can be produced by several methods with two general approaches, physicochemical and chemical, biosynthesis methods. Xia *et al.* reported the synthesis of cubic Ag nanocrystals in 2002.[11] Since then, Ag nanoparticles shaped like decahedrons[12] and bipyramids[13] have also been reported. Compared to nanoscale Ag materials with a spherical morphology, Ag nanoplates[14,15] show a number of advantages, such as a larger contact area and better electrical properties. Nano-Ag can be prepared by the liquid phase reduction method. However, it is difficult to purify and separate nano-Ag particles because of the small size and high surface energy. The common ways to clean metal nanoparticles include centrifugal separation,[16] ceramic membrane separation[17–20] and plasma cleaning. Nersisyan[21] and Sondi[22] both adopt high-speed settling centrifugal machine with more than 6000 rpm of centrifugal speed to purify and separate nano-Ag particles. It is found that the centrifugal separation is very distinct aggregation of nanoparticles and high energy consumption. Ceramic membrane separation, as a new physical separation technique, is usually used, but it's disadvantage is that the separation is incomplete.[23–25] Therefore, solid–liquid separation of Ag nanoparticles is a major technical problem for liquid phase method to achieve continuous production.

Graphene (GE) consists of carbon atoms tightly packed into a two-dimensional honeycomb lattice structure.[26–28] Electrons encounter very little resistance when traveling in GE. Thus, GE is used for nanometer-scale circuits.[29–33] However, most of these studies investigated only graphene oxide or the redox of graphene and metal nanoparticles.[34–36] However, because of these oxygen-bearing functional groups, lowering the conductivity of graphene oxide. There are a few reports on adding pure GE to nanometal-based conductive inks to improve the conductivity.[29,34]

In this study, nanohexagonal Ag platelets (AgNHPs) were prepared by using of liquid phase reduction method. Pure GE adopted is obtained using the liquid phase exfoliation method. Membrane separation technology and centrifugal cleaning are employed to purify the AgNHPs and remove the dispersing agent used during their synthesis and to decrease the contact resistivity of the AgNHPs and GE. The two materials are then used to synthesize a GE–AgNHPs conductive ink that exhibits self-assembly.[37] The electrical properties of the GE–AgNHPs

[a]*School of Materials Science and Engineering, Central South University, 410083 Changsha, China. E-mail: axlu@mail.csu.edu.cn; Fax: +86 731 22976365*
[b]*Hunan LEED Electronic Ink Co., Ltd, 412000 Zhuzhou, China*

conductive ink are also studied. Finally, the various factors influencing its performance as well as its underlying conduction mechanism are analyzed.

Experimental section

Materials

Polyvinylpyrrolidone (PVP K30), sodium hydroxide (NaOH), glucose, silver nitrate ($AgNO_3$), *N*-methyl pyrrolidone and anhydrous ethanol were purchased from Aladdin Industrial Corporation. GE was supplied by the Hunan Element Password Graphene Institute. All the chemicals were of analytical grade and were used without further purification. Deionized water was used in all experimental processes.

Syntheses of nanohexagonal Ag platelets (AgNHPs)

In a typical experimental procedure, silver nitrate was completely dissolved in 50 mL of deionized water to obtain a solution (0.35 mol L^{-1}). Next, PVP was dissolved in the aqueous silver nitrate solution in the same mass ratio. A NaOH solution (2 mol L^{-1}, 8 mL) was in a drop-wise manner to the resultant solution under ultrasonic agitation. After 30 min, the resulting solution was mixed with water at 60 °C under ultrasonication. Then, a glucose solution (4 mol L^{-1}, 8 mL) was added drop-wise to the resultant solution at a rate of 0.5 mL min^{-1} at 60 °C. After an ultrasonic treatment of 2 h, the reaction was considered complete, and the obtained AgNHPs were cleaned before being used to prepare the GE–AgNHPs ink.

Cleaning of AgNHPs solution

AgNHPs solution was cleaned by centrifugal separation, membrane separation and membrane separation-centrifugalization method respectively. Membrane cleaning equipment was provided by Jiangsu Jiuwu High-tech Company in China. The membrane tube number: JWCM19*30; outside diameter: 30 mm; inside: 4 mm; length: 1178 mm; membrane pore size: 50 nm. The centrifuge instrument was provided by Hunan instrument centrifuge instrument Co., Ltd, the unit type was L530, the maximum speed of revolution was 4200 rpm. The specific operations were as follows:

The obtained AgNHPs original fluid was marked as the sample A. The obtained AgNHPs original fluid (0.3 mol L^{-1}) was treated by diluting with deionized water in a ratio of 1 : 2, then diluents (50 mL each) were centrifugated at the rate of 4200 rpm for 1 h and liquid supernatant were removed and repeated for 3 times. To remove liquid supernatant, it were marked as the sample B.

The obtained AgNHPs solution was filtered using a split-ceramic membrane tube.[38] A circulating pump was used to result in cross-flow micro-filtration.[39,40] The cleaning process and equipment diagram was shown in Fig. 1, and the steps as follows: first, deionized water was added to the AgNHPs sol (1 L) in a 1 : 1 ratio. Deionized water was added when there was 1 L of the circulation fluid remaining. Next, 2 mL of the waste liquid was removed to add 2 mL of a HCl solution (1 mol L^{-1}) while using 2 mL of potassium dichromate (0.02 mol L^{-1}) as an indicator. The cleaning process was stopped until no sediment was observed. The cleaned samples were marked as the sample C.

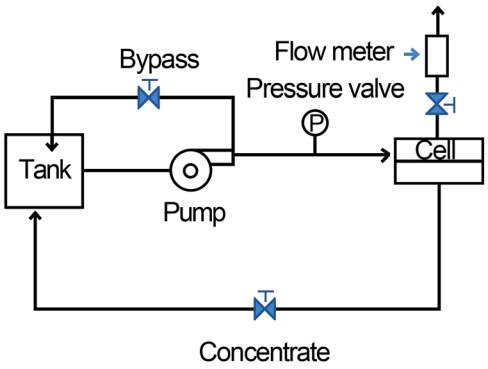

Fig. 1 The membrane separation process flow diagram.

The sample C (50 mL) with membrane cleaning was centrifugated at the rate of 4200 rpm for 1 h and liquid supernatant were removed. The centrifugates were marked as the sample D.

Ink preparation

The as-prepared AgNHPs were dispersed in *N*-methyl-pyrrolidone (NMP) in a concentration of 10 wt% using a sonicating bath. To form the GE–AgNHPs ink, the GE content was adjusted as follows:

NMP was added to a GE–NMP solution (0.5 mg mL^{-1}) in different amounts to obtain solutions with different concentrations (0.3 mg mL^{-1}, 0.15 mg mL^{-1}, 0.1 mg mL^{-1}, and 0.05 mg mL^{-1}). Then, 10 wt% of the total AgNHPs was added in each of the five GE–NMP solutions with different GE contents. The mixtures were subjected to ultrasonication for 1 h and then passed through a filter. The viscosity of the resultant ink was controlled to be 2–5 cp, while the surface tension was controlled to be 35–40 dyne cm^{-1}. It was confirmed that neither the AgNHPs nor the GE settled at the bottom after the inks had been left standing.

Fabrication of conductive films

The prepared ink was injected into a cartridge for use. Printing was done using an EPSON R300 printer with a 10 pL drop cartridge. The printing temperature was 30 °C. The prepared ink was printed on the glass wafers to form a rectangular pattern (0.6 cm × 5 cm). After the pattern had been printed on the substrates five times, after that, the printed substrates were placed into a dryer and sintered at different temperatures to form conductive films.

Characterization

The AgNHPs were analyzed using thermogravimetry analysis (TGA)-differential thermal analysis (Q50, TA Instruments, America). The test sample was tested from ambient temperature to 600 °C at a rate of 10 °C min^{-1}. The structure of the AgNHPs and GE were characterized using a field-emission scanning electron microscopy (FESEM) system (MIRA3, TESCAN, Czech

Republic). The dispersion were measured with a transmission electron microscopy system (JEOL-2100, Japan). The high voltage of scanning electron microscope (SEM HV) is 20.0 kV; working distance (WD) is 14.1 ± 0.1 mm. The changes in the heat flux during the fusion of the AgNHPs were observed using differential scanning calorimetry (DSC). The temperature was increased to 400 °C at a rate of 10 °C min^{-1}. The parameters used were the following: material: Ag; refractive index: 0.135; absorbance: 0.08; medium: water; temperature: 25 °C. The sheet resistances were determined using a four-point probe nanovoltmeter (ST2258C, Suzhou lattice electronic co., Ltd, China). The thicknesses of the conductive films were determined by scanning their cross-sections. These measurements were repeated 3 times at 25 °C, and the results were averaged. The Raman spectra of was measured using a Raman spectrometer (LabRAM HR800, Japan).

Results and discussion

Morphological and structural analysis

Fig. 2 shows the morphologies of the Ag nanoplates and the cleaning effect of different cleaning methods. As can be seen from Fig. 2a, most of the synthesized Ag nanoplates were hexagon. The strong and well-arrayed SAED spots shown in inset in Fig. 2a indicate the single-crystalline nature of the Ag nanoplates. Based on the corresponding SAED pattern obtained by projecting a diffraction beam along the {111} direction, it can be concluded that the flat and side faces of the AgNHPs were enclosed by {111} facets and {110} facets, respectively. The average thickness of the AgNHPs was approximately 10 nm. It can be observed that the particle sizes change from 20 nm to 80 nm (in Fig. 2e).

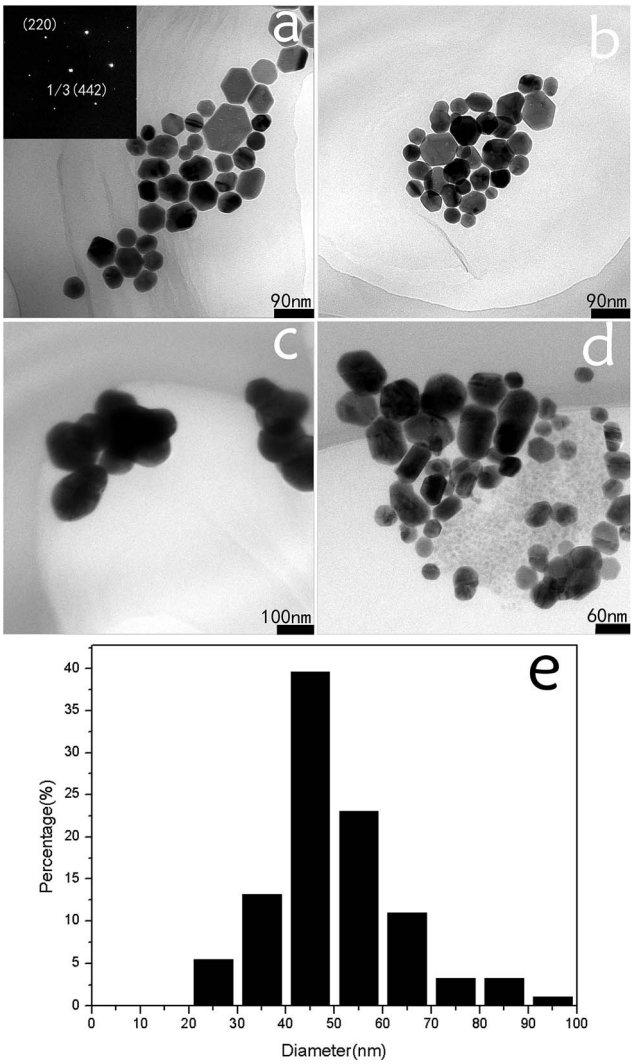

Fig. 2 TEM images of the AgNHPs cleaned by different method: (a) the sample A (AgNHPs original fluid); (b) the sample C, membrane tube (50 nm); (c) the sample B, 4200 rpm, 1 h, 3 times; (d) the sample D, membrane tube (50 nm); 4200 rpm, 1 h, once, (e) the particle size distribution histogram of AgNHPs.

Membrane separation cleaning process research and the cleaning effect from different cleaning method

The cleaning effects of centrifugal separation, membrane separation and membrane separation-centrifugation are compared in Fig. 3. Fig. 3a is the TGA image of the sample without cleaning. The weight loss between 180 °C and 300 °C is caused by the thermal decomposition of glucose, while the weight loss at 400 °C is owing to the thermal decomposition of PVP.

As shown in Fig. 3b, the sample treated with membrane separation did not show any noticeable weight loss before 350 °C, but there is decomposition of PVP at 400 °C. It proves that the residual organic material in the sample C with membrane separation is mainly PVP, and there is no lower-molecular organic residuals such as glucose. The AgNHPs content of sample C is about 80%.

This is because the ceramic membrane tube with 50 nm of pore diameter can filter most of lower-molecular organic residuals, but not those macromolecular impurities.[16] With certain pore diameter, it is hard for macromolecular to penetrate the ceramic membrane. The sample D was prepared using the ceramic membrane separation method to clean and remove most of lower-molecular organic materials, and then to treat AgNHPs with only once of centrifugal separation. In Fig. 3d, the loss weight of sample D is less than 5% at 600 °C. AgNHPs with small amounts of residuals can be obtained. The residual impurities are less than sample B and cleaning efficiency is higher. Therefore, the obtained AgNHPs has better dispersion effect after re-dispersion with ultrasonic treatment.

The morphologies of the AgNHPs that were separated and cleaned with different methods were also shown in Fig. 2. Fig. 2 shows the TEM images of sample A, B, C and D after re-dispersion. As shown in Fig. 2a, the AgNHPs in sample A shows clear dispersion effect without obvious agglomeration. A similar result is also obtained as shown in Fig. 2b for the AgNHPs with membrane separation treatment. It can be seen from Fig. 2c that there is obvious agglomeration after the sample experiencing many times of centrifugal separation. Compared to the dispersion effect as shown in Fig. 2c. The dispersion of AgNHPs

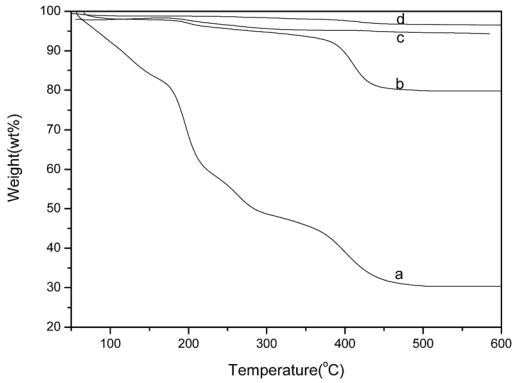

Fig. 3 TGA curves of the AgNHPs cleaned by different method: (a) the sample A (AgNHPs original fluid); (b) the sample C, membrane tube (50 nm); (c) the sample B, 4200 rpm, 1 h, 3 times; (d) the sample D, membrane tube (50 nm); 4200 rpm, 1 h, once.

in the sample D with membrane separation and then one-time centrifugation disperse is better, as seen in Fig. 2d.

Fig. 4 shows the morphologies of GE and GE–AgNHPs ink (GE: 0.15 mg mL^{-1}). Fig. 4a is an image of the GE material used to prepare the GE–AgNHPs conductive inks. As can be seen from the figure, the size of GE particles was relatively large and the GE sample did not exhibit multilayer stacking, indicating that, owing to good exfoliation, the GE sample was monolayered. The TEM image in the Fig. 4b is of the AgNHPs (sample B) on the surface of GE. The AgNHPs (sample D) on the surface of GE is also shown in Fig. 4c. Fig. 4d is a magnified version of the image in Fig. 4c and shows that most of AgNHPs were absorbed on the GE surface. It can be seen from Fig. 4b that there is obvious agglomeration of the sample B after the AgNHPs experiencing

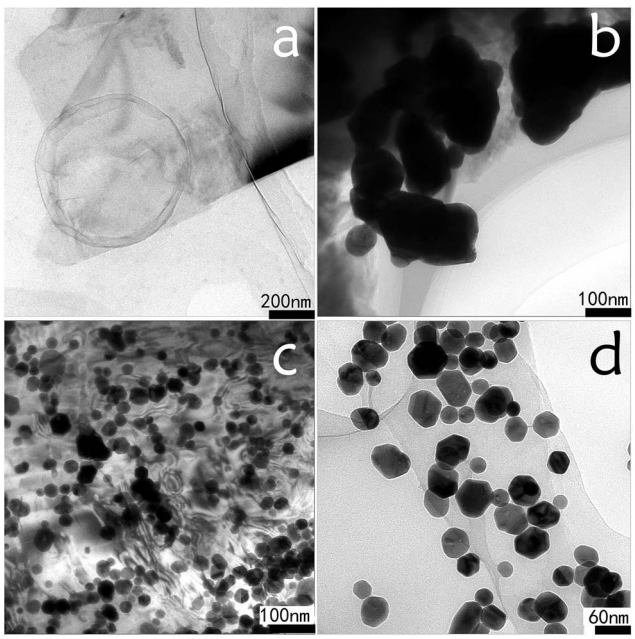

Fig. 4 TEM images of GE and GE–AgNHPs conductive ink. (a) GE; (b) the AgNHPs (sample B) on the surface of GE; (c) the AgNHPs (sample D) on the surface of GE; (d) magnified version of (c).

three times of centrifugal separation. This affects the interaction between AgNHPs and GE. As shown in Fig. 4c and d, the AgNHPs on the surface of GE shows clear dispersion effect without obvious agglomeration. This proved that the Ag nanoplates combined closely with the GE. The nanoparticles were arranged in an orderly manner on the GE surface, possibly owing to self-assembly.

The stability of nanocolloids depends mainly on electrostatic potential energy and van der Waals force among the colloid particles. Graphene oxide and GE can not only form ordered structures by self-assembly, but also show liquid crystalline properties when arranged by self-assembly.[27]

AgNHPs colloids cleaned with different method were printed by printer. Then the resistance of these samples sintered at different temperature was measured, respectively, as shown in Fig. 5. It can be seen from Fig. 5 that sample B prepared at 100 °C has poor conductive, and its electrical resistivity is about 5.8×10^{-2} Ω cm when the sintering temperature increases to 150 °C, at the same temperature, the electrical resistivity of sample D is 11.2×10^{-6} Ω cm. It is also found that the resistivity of sample B, C and D decrease with the increase of temperature. On one hand, the electrical conductivity of AgNHPs depends mainly on the connection degree between particles at low sintering temperature. With the increase of sintering temperature, the nanoparticles start to fuse because of surface effect, resulting in the decreasing of contact resistance. On the other hand, the PVP coated on the surface of AgNHPs prevents the contact among nanoparticles at low sintering temperature. With the increase of sintering temperature, the PVP start to melt which increases the surface of bare AgNHPs particles, causing the reducing of electrical resistivity. However, when PVP content is higher, it results in a higher electrical resistivity as sample C.

The sample D has low electrical resistivity because of lower PVP content and excellent contact among AgNHPs particles. Although sample B has small amounts of PVP, many times of centrifugation leads to the agglomeration of AgNHPs particles, which increases the average particle size and melting temperature of these particles. Thus, the electrical resistivity of sample B is not influenced obviously by sintering temperature.

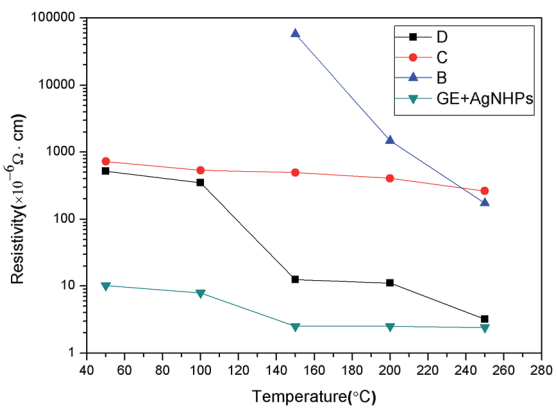

Fig. 5 The resistance of the AgNHPs cleaned by different method sintered on the glass substrate at different temperatures: the sample C, membrane tube (50 nm); the sample B: 4200 rpm, 1 h, 3 times; the sample D: membrane tube (50 nm); 4200 rpm, 1 h, once.

The electrical conductive performance of the GE–AgNHPs ink and the influence mechanism analysis

AgNHPs show many advantages, such as a large contact area between adjacent particles and good electrical properties. It was expected that the conductivity of the GE–AgNHPs conductive ink would be high. To observe the differences in the electrical conductivities of the various inks, patterns were printed on glass substrates using the AgNHPs ink and the GE–AgNHPs inks. The printed patterns were sintered at different temperatures for 30 min. The compositions and thicknesses of the sintered films are listed in Table 1.

The sheet resistivity is tested by a four-probe resistivity tester, and the relationship between resistivity value (ρ) of the conductive film, sheet resistivity (R_γ) and thickness (d) is $\rho = R_\gamma \times d$. The result are shown in Fig. 6.

As can be seen from the Fig. 6, the resistivity decreased as the sintering temperature was increased. Meanwhile, with an increase in the GE content, the resistivities at the different temperatures became approximate. The resistivity value of the AgNHPs ink was 5.2×10^{-4} Ω cm after sintering at 50 °C for 30 min (in Fig. 6).

When the sintering temperature was increased to 250 °C, the resistivity was the lowest, at 3.2×10^{-6} Ω cm. It was lower than the results reported in ref. 29 (at 3.6×10^{-6} Ω cm). This was because increasing the temperature resulted in the fusing of the nanoparticles. Similar to the case for the AgNHPs conductive ink, the resistivity of the film of (GE: 0.05 mg mL^{-1}) ink changed the most between 200 °C and 250 °C.

Table 1 Compositions and thicknesses of printed ink films after sintering

Number	GE content (mg mL^{-1})	Ag content (wt%)	Thickness of film (μm)
E	0	10	2.3
F	0.05	10	2.5
G	0.1	10	2.6
H	0.15	10	2.8
I	0.3	10	3.0
J	0.5	10	2.8

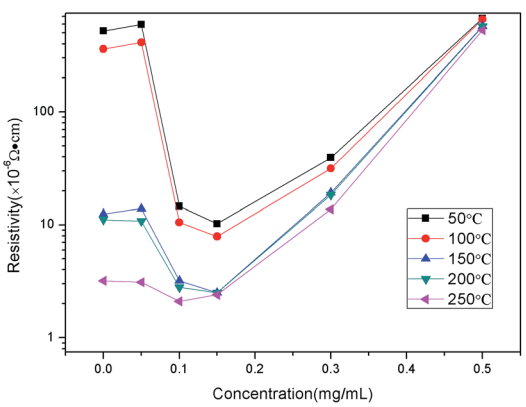

Fig. 6 Electrical properties of the GE–AgNHPs conductive inks with different GE contents.

This suggested that the Ag nanoparticles in the conductive ink were fused at 250 °C. The resistivity values of the films of the (GE: 0.1 mg mL^{-1} and 0.15 mg mL^{-1}) inks changed the most between 100 °C and 150 °C, indicating that the AgNHPs started to fuse together between 100 °C and 150 °C, in the presence of GE, the fused nanoparticles came into contact with the GE sheets as well. However, with a further increase in the GE content, the film conductivity depended mainly on the mutual overlapping of the GE sheets. Therefore, when the GE were 0.3 mg mL^{-1} and 0.5 mg mL^{-1}, it can be seen that temperature did not affect the resistance significantly.

A comparison of the electrical properties of the GE–AgNHPs conductive inks showed that the resistivity values of two of the ink samples (GE: 0.1 mg mL^{-1} and 0.15 mg mL^{-1}) were much lower than those of the others. This suggested that the addition of GE in a certain amount improves the electrical conductivity, especially when sintering is performed at a low temperature. Fig. 5 shows the electrical properties of the AgNHPs conductive ink and a GE–AgNHPs ink (GE: 0.15 mg mL^{-1}) after sintering at different temperatures. When sintering was performed at 150 °C, the resistivity of the GE–AgNHPs conductive ink (GE: 0.15 mg mL^{-1}) was 2.5×10^{-6} Ω cm, which is 13% of that of the AgNHPs ink and lower than that of the AgNHPs ink after sintering at 250 °C. It was lower than the results reported in ref. 29 (at 2.7×10^{-6} Ω cm). When sintering was performed at 50 °C, the resistivity of the GE–AgNHPs ink (10.2×10^{-6} Ω cm) was 2% of that of the AgNHPs ink (5.2×10^{-4} Ω cm) as shown in Fig. 6.

In order to observe the morphologies of the Ag layers formed, FESEM and DSC were used to characterize films of the AgNHPs conductive ink. Fig. 7a and b shows SEM images of the AgNHPs conductive ink after sintering at different temperatures for 30 min. As can be seen from Fig. 7a, the sample sintered at 150 °C, the formed Ag layer was distributed uniformly on the surface of substrate. The AgNHPs were connected together primarily, forming an agglomeration, at below the 150 °C. But it can also be seen from Fig. 7b that, as the sintering temperature was increased from 150 °C to 250 °C, the nanoparticles started to fuse together. Especially, significant interparticle sintering was observed at 250 °C, and most of the particles were fused with each other (Fig. 7b), and the resistivity of the AgNHPs films decreased markedly.

This was because the AgNHPs had a comparatively large surface energy and thus could be fused at temperatures lower than their melting temperature.

Fig. 8 shows the DSC curve of the AgNHPs samples sintered at 80–400 °C. A distinct endothermic peak can be seen between 125 °C. This is the melting peak of the Ag nanoparticle, it is caused by the surface effect of the Ag nanoparticles to melt at lower temperature than the melting point of Ag (960.8 °C). For a wider Ag nanoparticle size distribution (20–80 nm), the melting-related endothermic peak also widened. This result is in line with the results of the SEM analysis as well as the resistivity measurements.

This can be explained as follows: when a pattern was printed using the AgNHPs conductive ink, a few voids were produced, owing to its low stacking density. In particular, at low sintering temperatures, only a few AgNHPs formed contacts because of

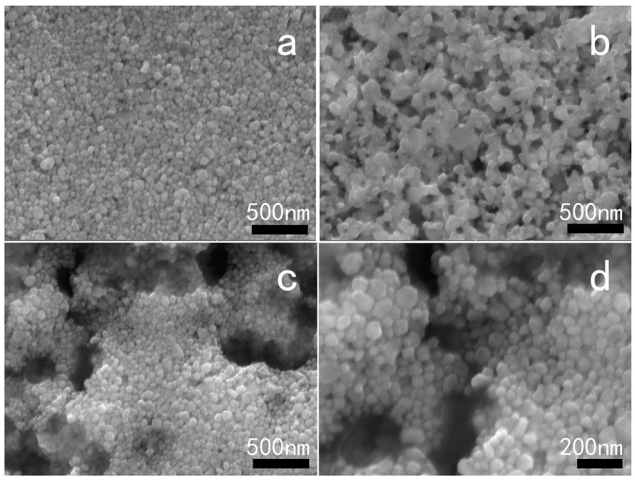

Fig. 7 SEM images of the AgNHPs and GE–AgNHPs inks with different GE contents after sintering. (a) AgNHPs at 150 °C/0.5 h; (b) AgNHPs at 250 °C/0.5 h; (c) the sample I, 150 °C/0.5 h; (d) the sample J, 150 °C/0.5 h and 220 °C.

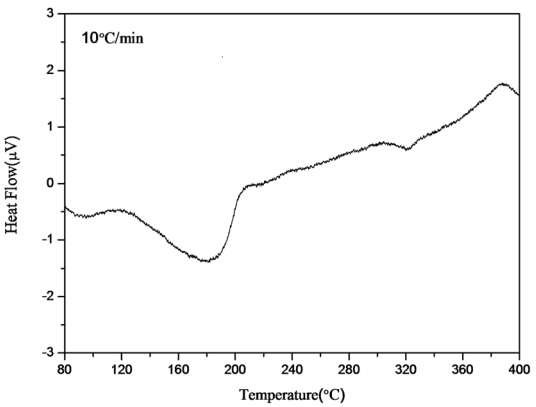

Fig. 8 DSC curve of the AgNHPs between 80 °C and 400 °C.

fusion; instead, most of them formed a conductive path because of stacking. As a result, the resistivity of the conductive ink coating was relatively high. On the other hand, when GE was added to the AgNHPs conductive ink, it filled the voids between the AgNHPs. Further, the AgNHPs were arranged in an orderly matter on the GE surface. This also improved the electrical performance of the ink. However, with the increase in the sintering temperature, more nanoparticles came into contact with each other. Hence, the effect of the GE weakened.

However, this does not mean that higher the GE content, the better the electrical properties of the conductive ink will be. When the GE content was 0.3 mg mL^{-1}, the resistivity of the ink was higher than that of the ink with a GE content of 0.15 mg mL^{-1}. Further, with an increase of the GE content to 0.5 mg mL^{-1}, the resistivity increased again. An SEM analysis was performed to compare the GE–AgNHPs inks after sintering at 150 °C, as shown in Fig. 7c and d.

This was because, with the increase in the GE content, a certain number of the Ag nanoparticles were adsorbed randomly onto the surface of the excess GE. This decreased the

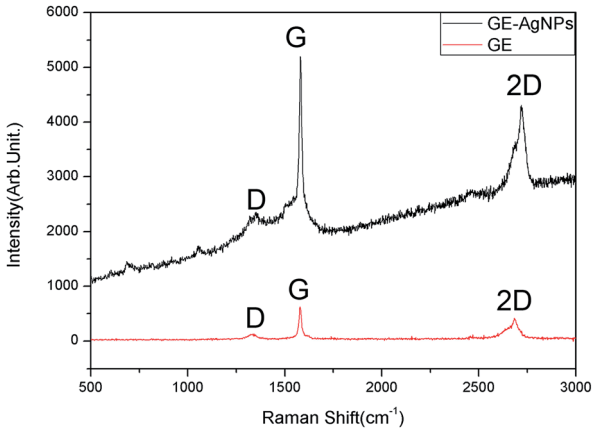

Fig. 9 The Raman spectra of GE and GE–AgNHPs in 530 nm excitation wavelength.

stacking density and lowered the extent of contact between the AgNHPs, as shown in Fig. 7a, the degrees of flatness and uniformity of the conductive films were higher without the GE. But, as shown in Fig. 7c and d when the GE contents were 0.3 mg mL^{-1} and 0.5 mg mL^{-1}, voids appeared and the films became uneven. Another reason is that, with the increase of the GE content, the amount of GE in the ink came closer to the saturation or supersaturation level, further affecting the ink's stability. Both AgNHPs and GE have high surface energies and cannot be uniformly dispersed in a high-concentration system. With the increase of sintering temperature, the solvent evaporated and the solids in the ink started to aggregate, causing voids to appear in the conductive films. Therefore, increasing the GE content beyond a certain threshold value lowered the conductivity of the coatings. But, when added in small amounts, GE can fill the voids between the AgNHPs. So, the resistivity of the conductive ink coatings decreases markedly at low temperatures.

The Raman spectra of GE and GE–AgNHPs in 530 nm excitation wavelength is shown in Fig. 9. The Raman peak at 1580 cm^{-1} is calculated for a clean G peak of graphene, This is made up of carbon atoms in the surface movement. The D peak is observed between 1340 and 1350 cm^{-1}, D peak and G peak intensity ratio (I_D/I_G) is the important indicators of graphene irregular degree and order.[33] It can be found from Fig. 9 that the Raman spectra of GE–AgNPs is significantly enhanced when graphene composite with AgNHPs. This is consistent with the result from literatures,[33] which has obvious SERS effect after AgNHPs compositing with GE. The interaction of graphene with functional groups in the end of the molecular plays an important role for SERS effect. The enhanced Raman spectra powerful proved that it exists a relatively close interaction between AgNHPs and graphene. This is conducive to uniform distribution of the silver nanoparticles on the surface of graphene. Certainly, it is also conducive to decrease the resistivity of the GE–AgNHPs.

Conclusions

In this study, single-crystal nanohexagonal Ag platelets were prepared by liquid phase reduction method. The different

treatment processes for AgNHPs solution were studied. It was found that high dispersity and low electrical resistivity of AgNHPs solution can be obtained by using membrane separation-centrifugation method. The sample prepared at 150 °C has excellent low electrical resistivity until 11.2×10^{-6} Ω cm. However, the electrical resistivity of the samples cleaned by the membrane separation and centrifugation respectively is about 8×10^{-4} Ω cm and 5.8×10^{-2} Ω cm at the same temperature, respectively. Then, the GE–AgNHPs conductive ink was produced through ultrasonic dispersion. The low-energy {111} plane of the AgNHPs caused them to get arranged in an orderly manner on the GE surface. As a result, the ink based on them showed good electrical conductivity. Further, it was found that the addition of GE reduced the resistivity of the ink at low sintering temperatures. The resistivity of the GE–AgNHPs conductive ink with a GE content of 0.15 mg mL^{-1} was the lowest and was found to be 2.5×10^{-6} Ω cm after sintering at 150 °C, this is 13% of that of the AgNHPs conductive ink. It was lower than the results reported in ref. 29 (at 2.7×10^{-6} Ω cm). On the other hand, after sintering at 50 °C, the resistivity of the GE–AgNHPs conductive ink was 2% of that of the AgNHPs conductive ink. It is proved by the enhanced Raman spectra powerful that it exists a relatively close interaction between AgNHPs and graphene. This is conducive to uniform distribution of the AgNHPs on the surface of graphene. Certainly, it is also conducive to decrease the resistivity of the GE–AgNHPs.

Thus, a holistic approach for producing highly conductive GE–AgNHPs conductive inks that can be sintered at low temperatures was demonstrated. Such inks will be widely used in flexible circuit.

Acknowledgements

This work was supported by the International S&T Cooperation Special Funds Plan (Grant No. 2015DFI53030) of China.

Notes and references

1 T. T. Nge, M. Nogi and K. Suganuma, Electrical functionality of inkjet-printed silver nanoparticle conductive tracks on nanostructured paper compared with those on plastic substrates, *J. Mater. Chem. C*, 2013, **1**(34), 5235–5243.

2 L. Xu, H. Li, J. Xia, L. Wang and H. Xu, Graphitic carbon nitride nanosheet supported high loading silver nanoparticle catalysts for the oxygen reduction reaction, *Mater. Lett.*, 2014, **128**(6), 349–353.

3 W. Li, T. Wu, R. Jiao, B. P. Zhang, S. Li, *et al.*, Effects of silver nanoparticles on the firing behavior of silver paste on crystalline silicon solar cells, *Colloids Surf., A*, 2015, **466**(466), 132–137.

4 A. C. Siegel, S. T. Phillips, M. D. Dickey1, N. Lu, Z. Suo and G. M. Whitesides, Foldable Printed Circuit Boards on Paper Substrates, *Adv. Funct. Mater.*, 2010, **20**, 28–35.

5 Y. Chen, J. Au, P. Kazlas, A. Ritenour, H. Gates and M. McCreary, Flexible active-matrix electronic ink display, *Nature*, 2003, **423**, 136–137.

6 T. H. J. van Osch, J. Perelaer, A. W. M. de Laat and U. S. Schubert, Inkjet Printing of Narrow Conductive Tracks on Untreated Polymeric Substrates, *Adv. Mater.*, 2008, **20**, 343–345.

7 W. Xu, J. Zhao, *et al.*, Sorting of large-diameter semiconducting carbon nanotube and printed flexible driving circuit for organic light emitting diode (OLED), *Nanoscale*, 2014, **6**, 1589–1595.

8 B. Y. Ahn, E. B. Duoss, M. J. Motala, X. Guo, S. l. Park, Y. Xiong, J. Yoon, R. G. Nuzzo, J. A. Rogers and J. A. Lewis, Omnidirectional printing of flexible, stretchable, and spanning silver microelectrodes, *Science*, 2009, **323**(5921), 1590–1593.

9 K. Chi, Z. Zhang, J. Xi, Y. Huang, F. Xiao, S. Wang and Y. Liu, Freestanding graphene paper supported three-dimensional porous graphene–polyaniline nanocomposite synthesized by inkjet printing and in flexible all-solid-state supercapacitor, *ACS Appl. Mater. Interfaces*, 2014, **6**, 16312.

10 F. Xiao, S. Yang, Z. Zhang, H. Liu, J. Xiao, L. Wan, J. Luo, S. Wang and Y. Liu, Scalable Synthesis of Freestanding Sandwich-structured Graphene/Polyaniline/Graphene Nanocomposite Paper for Flexible All-Solid-State Supercapacitor, *Sci. Rep.*, 2015, **5**, 9359.

11 Y. G. Sun and Y. N. Xia, Shape-Controlled Synthesis of Gold and Silver Nanoparticles, *Science*, 2002, **298**(5601), 2176–2179.

12 Y. Gao, P. Jiang, L. Song, *et al.*, Studies on silver nanodecadrons synthesized by PVP-assisted *N*,*N*-dimethylformamide (DMF) reduction, *J. Cryst. Growth*, 2006, **289**, 376–380.

13 B. J. Wiley, Y. J. Xiong, Y. N. Xia, *et al.*, Right bipyramids of silver: a new shape derived from single twinned seeds, *Nano Lett.*, 2006, **6**, 765–768.

14 L. M. Gilbertson, J. B. Zimmerman, *et al.*, Designing nanomaterials to maximize performance and minimize undesirable implications guided by the principles of green chemistry, *J. Mater. Chem.*, 2015, **44**, 5758–5777.

15 I. Pastoriza-Santos and L. M. Liz-Marzan, Synthesis of Silver Nanoprisms in DMF, *Nano Lett.*, 2002, **2**, 1565.

16 L. Bai, X. Ma, J. Liu, X. Sun, D. Zhao, *et al.*, Rapid separation and purification of nanoparticles in organic density gradients, *J. Am. Chem. Soc.*, 2010, **132**(7), 2333–2337.

17 B. Rajaeian, A. Rahimpour, M. O. Tade and S. Liu, Fabrication and characterization of polyamide thin film nanocomposite (TFN) nanofiltration membrane impregnated with TiO_2 nanoparticles, *Desalination*, 2013, **313**(7), 167–188.

18 V. Vatanpour, S. S. Madaeni, A. R. Khataee, E. Salehi, *et al.*, TiO_2 embedded mixed matrix PES nanocomposite membranes: influence of different sizes and types of nanoparticles on antifouling and performance, *Desalination*, 2012, **292**(9), 19–29.

19 J. E. Zhou, Q. Chang, Y. Wang, J. Wang and G. Meng, Separation of stable oil–water emulsion by the hydrophilic nano-sized ZrO_2 modified Al_2O_3 microfiltration membrane, *Sep. Purif. Technol.*, 2010, **75**(3), 243–248.

20 H. Park, Y. Kim, B. An and H. Choi, Characterization of natural organic matter treated by iron oxide nanoparticle

incorporated ceramic membrane-ozonation process, *Water Res.*, 2012, **46**(18), 65–68.

21 H. H. Nersisyan, J. H. Lee, H. T. Son, C. W. Won and D. Y. Maeng, A new and effective chemical reduction method for preparation of nanosized silver powder and colloid dispersion, *Mater. Res. Bull.*, 2003, **38**(6), 949–956.

22 I. Sondi and B. Salopek-Sondi, Silver nanoparticles as antimicrobial agent: a case study on *E. coli* as amodel for Gram-negative bacteria, *J. Colloid Interface Sci.*, 2004, **275**(1), 177–182.

23 B. V. D. Bruggen, Integrated Membrane Separation Processes for Recycling of Valuable Wastewater Streams: Nanofiltration, Membrane Distillation, and Membrane Crystallizers Revisited[J], *Ind. Eng. Chem. Res.*, 2013, **52**(31), 10335–10341.

24 M. T. M. Pendergast and E. M. V. Hoek, A review of water treatment membrane nanotechnologies, *Energy Environ. Sci.*, 2011, **4**(6), 1946–1971.

25 C. Charcosset, R. Kieffer, D. Mangin and F. Puel, Coupling Between Membrane Processes and Crystallization Operations, *Ind. Eng. Chem. Res.*, 2010, **49**(12), 5489–5495.

26 I. V. Grigorieva, K. S. Novoselov, A. K. Geim, *et al.*, Electric Field Effect in Atomically Thin Carbon Films, *Science*, 2004, **306**(5696), 666–669.

27 K. S. Novoselov, E. Mccann, S. V. Morozov, V. I. Fal'Ko, *et al.*, Unconventional quantum Hall effect and Berry's phase of 2π in bilayer graphene, *Nat. Phys.*, 2006, **2**, 177–180.

28 T. Y. Kim, S. W. Kwon, S. J. Park, *et al.*, Self-organized graphene patterns, *Adv. Mater.*, 2011, **23**, 2734–2738.

29 P. Liu, J. Ma, S. Deng, K. Zeng, D. Y. Deng, W. Xie and A. X. Lu, Graphene–Ag nanohexagonal platelets-based ink with high electrical properties at low sintering temperatures, *Nanotechnology*, 2016, **27**, 385603.

30 Y. H. Kim, B. Yoo, J. E. Anthony and S. K. Park, Controlled Deposition of a High Performance Small Molecule Organic Single Crystal Transistor Array by Direct Ink Jet Printing, *Adv. Mater.*, 2012, **24**(4), 497–502.

31 J. Li, F. Ye, S. Vaziri, M. Muhammed, *et al.*, Efficient Inkjet Printing of Graphene, *Adv. Mater.*, 2013, **25**(29), 3985–3992.

32 L. Zhang, H. Liu, Y. Zhao, X. Sun, *et al.*, Inkjet Printing High-Resolution, Large-Area Graphene Patterns by Coffee-Ring Lithography[J], *Adv. Mater.*, 2012, **24**(3), 436–440.

33 L. Li, Y. Guo, X. Zhang and Y. Song, Inkjet-printed highly conductive transparent patterns with water based Ag-doped graphene, *J. Mater. Chem. A*, 2014, **2**(44), 19095–19101.

34 J. Liu, Y. Hu, Y. Zhang and W. Chen, Graphene-Stabilized Silver Nanoparticle Electrochemical Electrode for Actuator Design, *Adv. Mater.*, 2013, **25**, 1270–1274.

35 X.-Y. Dong, Zi-W. Gao, *et al.*, Nanosilver as a new generation of silver catalysts in organic transformations for efficient synthesis of fine chemicals, *J. Mater. Chem.*, 2015, **5**, 2554–2574.

36 Y. Xu, Q. Wu, Y. Sun, *et al.*, Three-dimensional self-assembly of graphene oxide and DNA into multifunctional hydrogels, *ACS Nano*, 2010, **4**(10), 7358–7362.

37 T. Y. Kim, S. W. Kwon, S. J. Park, *et al.*, Self-organized graphene patterns, *Adv. Mater.*, 2011, **23**, 2734–2738.

38 M. C. Adams and D. M. Barbano, Effect of ceramic membrane channel diameter on limiting retentate protein concentration during skim milk microfiltration, *J. Dairy Sci.*, 2015, **99**(1), 167–182.

39 M. Darius, R. Laimonas, S. Robert and L. J. V. Zenonas, Optimization of Crossflow Microfiltration of Disrupted Arthrobacter Luteus Cells, *Sep. Sci. Technol.*, 2015, **50**(11), 1709–1720.

40 S. T. Kang, A. Subramani, E. M. V. Hoek, M. A. Deshusses and M. R. Matsumoto, Direct observation of biofouling in cross-flow microfiltration: mechanisms of deposition and release, *J. Membr. Sci.*, 2004, **244**(1–2), 151–165.